



UNIVERSITY OF LEEDS

This is a repository copy of *Dielectric properties of liquid crystalline dimer mixtures exhibiting the nematic and twist-bend nematic phases*.

White Rose Research Online URL for this paper:
<http://eprints.whiterose.ac.uk/123381/>

Version: Accepted Version

Article:

Trbojevic, N orcid.org/0000-0001-7385-2579, Read, D orcid.org/0000-0003-1194-9273 and Nagaraj, M orcid.org/0000-0001-9713-1362 (2017) Dielectric properties of liquid crystalline dimer mixtures exhibiting the nematic and twist-bend nematic phases. *Physical Review E - Statistical, Nonlinear, and Soft Matter Physics*, 96 (5). 052703. ISSN 1539-3755

<https://doi.org/10.1103/PhysRevE.96.052703>

© 2017 American Physical Society. This is an author produced version of a paper published in *Physical Review E*. Uploaded in accordance with the publisher's self-archiving policy.

Reuse

Unless indicated otherwise, fulltext items are protected by copyright with all rights reserved. The copyright exception in section 29 of the Copyright, Designs and Patents Act 1988 allows the making of a single copy solely for the purpose of non-commercial research or private study within the limits of fair dealing. The publisher or other rights-holder may allow further reproduction and re-use of this version - refer to the White Rose Research Online record for this item. Where records identify the publisher as the copyright holder, users can verify any specific terms of use on the publisher's website.

Takedown

If you consider content in White Rose Research Online to be in breach of UK law, please notify us by emailing eprints@whiterose.ac.uk including the URL of the record and the reason for the withdrawal request.



eprints@whiterose.ac.uk
<https://eprints.whiterose.ac.uk/>

Dielectric properties of liquid crystalline dimer mixtures exhibiting the nematic and twist-bend nematic phases

Nina Trbojevic¹, Daniel J. Read², Mamatha Nagaraj^{1*}

School of Physics and Astronomy, University of Leeds, Leeds LS2 9JT, UK

School of Mathematics, University of Leeds, Leeds LS2 9JT, UK

*Corresponding author: m.nagaraj@leeds.ac.uk

A detailed investigation of the thermal and dielectric properties of a series of binary mixtures exhibiting the nematic (N) and twist-bend nematic (N_{TB}) liquid crystal phases is presented. The mixtures consist of an achiral, dimeric liquid crystal CB7CB, which forms the nematic and twist-bend nematic phases, and a calamitic liquid crystal 5CB, which shows the nematic phase. As the concentration of the calamitic liquid crystal is increased, the transition temperatures decrease linearly, and the width of the nematic phase increases. The enthalpies of phase transitions obtained from DSC measurements show that on increasing the concentration of 5CB in the binary mixtures, the enthalpy associated with the N to N_{TB} phase transitions reduces considerably compared to a clear first order N- N_{TB} transition in pure CB7CB. The real and imaginary parts of the dielectric permittivity are measured as a function of frequency from 100 Hz to 2 MHz in the nematic and twist-bend nematic phases in planar and homeotropic devices. A significant decrease in the average dielectric permittivity as a function of temperature for mixtures forming the N_{TB} phase is observed. Measurements of the imaginary part of the dielectric permittivity show a relaxation peak in the measured frequency window for all of the mixtures exhibiting the N_{TB} phase. The activation energy associated with this relaxation process is calculated and is shown to remain constant irrespective of the composition of the mixtures.

I. INTRODUCTION

Liquid crystals are a state of matter that exist between conventional solids and isotropic liquids. The simplest liquid crystalline phase is the nematic phase. In the nematic phase, the mesogens exhibit orientational order along a direction known as the director, \mathbf{n} . One of the important findings of recent years is the discovery of a second nematic phase, known as the twist-bend nematic (N_{TB}) phase [1–11]. In the twist-bend nematic phase, in addition to the orientational order, the mesogens spontaneously self-assemble into a helical structure having a pitch length of the order of a few nanometers [12,13]. The way in which the helical structure is achieved is through the simultaneous twisting and bending of the director in space, hence the name ‘twist-bend’ nematic (Figure 1) [14]. It is remarkable that in the twist-bend nematic phase the helical structure is spontaneously generated and the phase exhibits degenerate domains of opposite handedness, even though the constituent molecules are achiral in nature [15,16]. The helical structure is also associated with a temperature-dependent tilt angle – the angle between the director and the helical axis – which can range up to about 30° [6,13]. Twist-bend nematic liquid crystals have attracted a great deal of attention for a number of reasons, including high flexoelectric effect [17,18] and ultra-fast response times, making them promising for applications in fast-switching photonic and electro-optic devices. A recent paper [19] reporting a sub-millisecond electro-optic switching time of a dimer exhibiting the N_{TB} phase suggests the prospects of these materials for application in 3D liquid crystal displays and as active retarders for quantum computing.

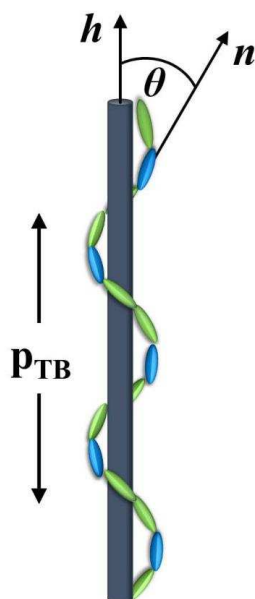


Figure 1

The twist-bend nematic phase has been observed in molecules of various architecture, including dimers [4,20,21] and bent-core liquid crystals [22,23]. Dimeric liquid crystals consist of two mesogenic units linked together via a flexible spacer. The nature, length and parity of the flexible spacer decide the angle between the two mesogenic units and hence the conformation of the dimer [20]. Dielectric properties have been previously studied for pure dimeric liquid crystals of both positive and negative dielectric anisotropies that exhibit the twist-bend nematic phase [24–26]. Dielectric spectroscopy measures the dielectric properties

of a material, such as relaxation processes occurring within molecules, as a function of frequency. It is an excellent technique to probe conformational distribution and changes in liquid crystalline structures. Variation in conformations and their population distribution gives an insight into the molecular shape of the liquid crystal, which is an important feature in determining phase behaviour and physical properties [15,27–33]. This is based on the principle that a change in the molecular conformation would change the mean-square dipole moment, which provides a direct link to the molecular shape. The mean-square dipole moment is an averaged vector sum of dipoles. For dimeric liquid crystals having terminal polar groups on the mesogenic units, a change in the molecular shape or orientation of the liquid crystal would result in variation of the direction and magnitude of the dipole moment. This would in turn affect the dielectric anisotropy of the material. For liquid crystal phases, two components of the dielectric permittivity (perpendicular and parallel) can be measured over a range of frequencies, which allows for the mean-square dipole moment to be measured perpendicular and parallel to the applied electric field.

In this paper a systematic investigation of the thermal and dielectric properties of a series of binary mixtures consisting of the dimeric liquid crystal CB7CB and the calamitic liquid crystal 5CB is presented. The CB7CB liquid crystal exhibits nematic and twist-bend nematic phases, whereas 5CB exhibits a nematic phase. A complete phase diagram of CB7CB and 5CB mixtures is provided with a detailed investigation of the phase transition temperatures and transition enthalpies carried out by differential scanning calorimetry. The real and imaginary parts of the dielectric permittivity are measured as a function of frequency from 100 Hz to 2 MHz for both planar and homeotropic alignment of the liquid crystal director and the activation energies of molecular relaxations are calculated.

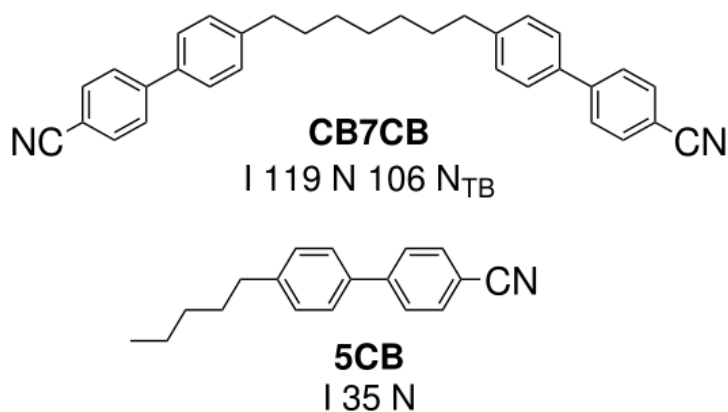


Figure 2

II. EXPERIMENTAL

A series of binary mixtures was prepared by mixing varying concentrations by weight (wt%) of 1'',7''-bis(4-cyanobiphenyl-4'-yl)heptane (CB7CB; purchased from SYNTHON Chemicals, Germany) with 4-cyano-4'-pentylbiphenyl (5CB, purchased from Sigma Aldrich). The chemical structure of the two liquid crystals is given in Figure 2.

Dielectric spectroscopy measurements were performed using an Agilent E4980A Precision LCR Meter. Devices of 10 μm spacing (AWAT PPW, Poland) having an indium tin oxide (ITO) electrode layer of sheet resistance $15\Omega/\square$ were filled with the liquid crystals in their nematic phase, and then glue-sealed. Measurements of dielectric permittivity were performed by heating the sample to the isotropic state and cooling down at a rate of $0.5\text{ }^\circ\text{C min}^{-1}$.

The real (ϵ') and imaginary (ϵ'') parts of the dielectric permittivity were measured at $0.1 V_{\text{RMS}}$ and $20 V_{\text{RMS}}$ (corresponding to planar and homeotropic alignment of the director, respectively) as a function of frequency from 100 Hz to 2 MHz. A uniform planar alignment has been obtained in the nematic phase for both pure materials and the mixtures for the dielectric experiments. More details on the textures seen in the N_{TB} phase are given in the ‘polarising optical microscopy’ section. Obtaining spontaneous homeotropic alignment in the twist-bend nematic phase is challenging. The homeotropic alignment mentioned here was uniform and optically dark (no transmission in the high field state) between crossed polarisers for both the nematic and N_{TB} phases for all the materials across the phase diagram. The static nature of the dark state has also been checked to make sure of absence of electro-convection. The homeotropic permittivity can also be obtained by extrapolating the permittivity measured as a function of applied voltage in a planar device through $1/\text{Voltage}$ extrapolation. Voltages between $0.1 V_{\text{RMS}}$ and $20 V_{\text{RMS}}$ were continuously applied to the device, whereby the permittivities obtained at 10 kHz were then extrapolated to obtain a permittivity at infinite voltage. A comparison of the permittivity measured in the homeotropic geometry of the nematic phase and by $1/\text{Voltage}$ extrapolation gave values within ± 0.5 .

In order to obtain the dielectric strength and relaxation frequency of the relaxation processes, the dielectric loss was fitted to the Havriliak-Negami equation [34]:

$$\epsilon^*(\omega) = \epsilon' - i\epsilon'' = \epsilon_\infty + \sum_{k=1,2} \frac{\Delta\epsilon_k}{[1 + (i\omega\tau_k)^{\alpha_k}]^{\beta_k}} - \frac{i\sigma_{DC}}{\omega\epsilon_0}$$

where $\omega = 2\pi f$ (f is the frequency in Hz) and ϵ_0 is the permittivity of free space, ϵ_∞ is the permittivity at the high-frequency limit, $\Delta\epsilon_k$ is the strength of the relaxation mode and σ_{DC} is the DC conductivity. The relaxation time is characterised by τ_k and the parameters α_k and β_k describe the shape of the spectra. For a Debye relaxation $\alpha = \beta = 1$, and for a Cole-Cole distribution $\alpha < 1$ and $\beta = 1$ [34].

The polarising optical microscopy (POM) experiments were carried out using a Leica DM2700P polarisation microscope. A Linkam THMS600 hot stage connected to a Linkam T95-PE temperature controller was used to control the sample temperature. Phase transition temperatures were determined by cooling the samples at $0.1\text{ }^\circ\text{C min}^{-1}$.

For differential scanning calorimetry (DSC) experiments, a DSC Q20 V24.11 Build 124 was used. Heating and cooling cycles were performed at a constant rate of $10\text{ }^\circ\text{C min}^{-1}$. The phase transition peaks were integrated to obtain the associated enthalpies (ΔH in kJmol^{-1}) of transition. Enthalpies of the phase transitions for a particular onset temperature were calculated using the latent heat (Jg^{-1}) given in the DSC graphs and the molar mass of the

materials. Dimensionless entropies of phase transitions ($\Delta S/R$) were calculated using the transition enthalpies ΔH , onset temperatures and the gas constant R .

III. RESULTS AND DISCUSSION

A. Phase diagram of the binary mixtures of CB7CB and 5CB liquid crystals

The chemical structures and transition temperatures of CB7CB and 5CB liquid crystals are given in Figure 2. CB7CB consists of two rigid cyanobiphenyl mesogenic units linked via a flexible methylene spacer. The cyano- groups lie along the long molecular axes of the two mesogenic units and they are the largest contributors to the total dipole moment of the liquid crystal. 5CB is a monomeric liquid crystal having a similar molecular structure to that of the monomer of CB7CB. A series of binary mixtures of CB7CB with 5CB were prepared to understand the influence of the calamitic liquid crystal 5CB on phase transition temperatures and on the stability of the N_{TB} phase. Previously, a detailed investigation by freeze-fracture transmission electron microscopy had been made on similar binary mixtures [11]. Figure 3 depicts the phase diagram obtained for CB7CB by means of polarising optical microscopy where the transition temperatures are comparable to those reported in reference [11]. As the concentration of 5CB increases, the phase diagram clearly shows a linear decrease in the isotropic to nematic and the nematic to twist-bend nematic phase transition temperatures as well as an increase in the width of the nematic phase. The mixtures were carefully investigated by POM (more details are provided later) to check for any visible phase separation, however, no noticeable immiscibility of the two liquid crystals is observed across the phase diagram.

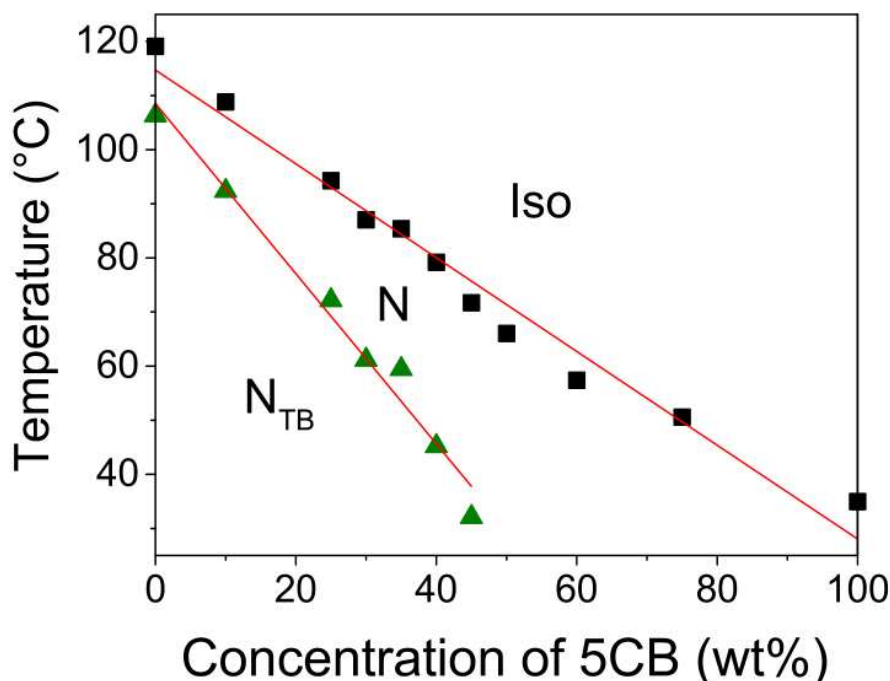


Figure 3

B. Differential scanning calorimetry

Table 1 lists the phase transition temperatures of pure CB7CB and 5CB liquid crystals and their mixtures, obtained using polarising optical microscopy (POM), as well as phase transition enthalpies (ΔH) obtained from the second cooling cycle of differential scanning calorimetry (DSC) experiments. Representative DSC curves of pure materials and mixtures **M35**, **M40** and **M50** are provided in the supplemental material [35]. Crystallisation temperatures are not reported for CB7CB nor for the binary mixtures as the samples tend to supercool. The melting point of 102 °C [13] reported for CB7CB is the temperature obtained on heating the sample from the crystalline state.

Table 1: List of transition temperatures (obtained by polarising optical microscopy experiments) and enthalpies of phase transition (determined using differential scanning calorimetry) for the CB7CB/5CB binary mixtures. I – isotropic, N – nematic, N_{TB} – twist-bend nematic phase, ΔH – enthalpy of 2nd cooling cycle at a cooling rate of 10 °C min⁻¹. Values that were not measurable are represented with a dash (-).

Compound	5CB (wt%)	T_{NI} (°C)	ΔH (kJ/mol)	T_{N-NTB} (°C)	ΔH (kJ/mol)
CB7CB	0	119.09	0.90	106.33	1.19
M10	10	108.83	0.68	92.37	0.46
M25	25	94.25	0.62	72.16	0.18
M30	30	87.03	0.69	61.17	0.16
M35	35	85.39	0.50	59.43	no peak
M40	40	79.18	0.60	45.19	no peak
M45	45	71.70	0.26	32.10	no peak
M50	50	66.03	0.46	-	-
M60	60	57.39	0.55	-	-
M75	75	50.57	0.71	-	-
5CB	100	34.97	0.58	-	-

The DSC curve of CB7CB shows a clear first order N-N_{TB} phase transition with an enthalpy of 1.19 kJ mol⁻¹. Furthermore, the magnitude of heat capacity for the N-N_{TB} transition in CB7CB is higher than that of other dimeric liquid crystals which exhibit the twist-bend nematic phase [9]. It is to be noted that in pure CB7CB, the enthalpy of the isotropic to nematic transition (0.90 kJ mol⁻¹) is slightly lower than the N to N_{TB} transition (1.19 kJ mol⁻¹). This was also the case for the second heating cycle, in which the enthalpies of the N-Iso and N_{TB}-N transitions were 0.75 kJ mol⁻¹ and 0.92 kJ mol⁻¹, respectively. The pure CB7CB liquid crystal has been investigated by DSC before and the enthalpy of phase transition mentioned in this paper are comparable to previous studies [36,37].

Figure 4 shows plots of enthalpy and entropy (inset) of the Iso-N and N-N_{TB} phase transitions as a function of concentration for the binary mixtures. As the concentration of 5CB increases, on the left hand side of the diagram in Figure 4, the Iso-N enthalpies decrease from being 0.90 kJ mol⁻¹ for pure CB7CB, to 0.26 kJ mol⁻¹ for 45 wt% of 5CB in CB7CB. The corresponding entropies of Iso-N phase transitions given as an inset in Figure 4 also show a similar trend from 0.28 (for pure CB7CB) to 0.09 (for the 45 wt% 5CB in CB7CB mixture). On the right hand side of the enthalpy and entropy diagrams, as the concentration of 5CB increases, an increase in both the enthalpy and entropy of the phase transition is observed. It is important to emphasise that, as the concentration of 5CB increases, the energies associated with the N-N_{TB} phase transition are reduced significantly from being 1.19 kJ mol⁻¹ for pure CB7CB, to 0.16 kJ mol⁻¹ for **M30** (30 wt% of 5CB in CB7CB) as shown in Figure 4. The corresponding entropy of the N-N_{TB} transition also decreases from 0.38 for pure CB7CB, to 0.06 for 30 wt% 5CB in CB7CB (Figure 4 inset). It is to be noted that when the concentration of 5CB is increased beyond 30 wt%, no measurable enthalpies for the N-N_{TB} transition were observed: mixtures **M35**, **M40** and **M45** do not show a clear, discernible N-N_{TB} transition peak in their DSC curves (for the DSC curves of mixtures **M35** and **M40**, see supplemental material [35]). However, in all these mixtures, at the N-N_{TB} phase transition, clear textural changes having a sharp boundary between the nematic and twist-bend nematic phase with focal conic and rope-like textures characteristic of the N_{TB} phase are observed using polarising optical microscopy. This implies that as the concentration of 5CB liquid crystal is increased in the binary mixtures, the entropy associated with the N-N_{TB} phase transition decreases or the energy difference between the two phases decreases, as opposed to a clear first order N to N_{TB} transition in pure CB7CB. On further increasing the 5CB concentration (≥ 50 wt%), the mixtures exhibit only the nematic phase till room temperature and the enthalpies of which shows a slight increase (**M50**, **M60** and **M75** in Table 1, and Figure 4). Further, the enthalpy of the Iso-N transition in **M50** is 0.12 kJ mol⁻¹ lower than that in pure 5CB. This might be due to the fact that in comparison to the sharper Iso-N transition peak observed for 5CB, where the width of the peak $\Delta T = 6$ °C, the DSC curve of **M50** shows a broad Iso-N transition peak with $\Delta T = 10$ °C (ΔT is the difference in the two temperatures between which the transition peak is integrated to obtain enthalpy values). Mixture **M60** also shows a broad isotropic to nematic transition peak having $\Delta T = 13$ °C.

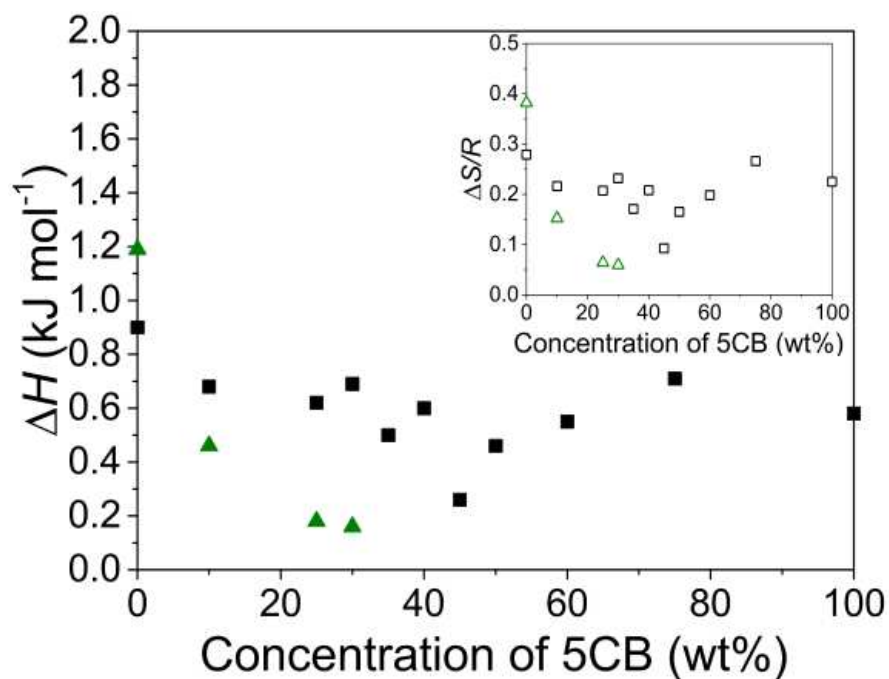


Figure 4

C. Polarising optical microscopy

Figure 5 shows the polarising optical microscopy (POM) textures of CB7CB liquid crystal in the nematic and twist-bend nematic phases when cooled from the isotropic phase and viewed between untreated glass substrates. The nematic phase exhibits schlieren textures, having 2- and 4-brush defects (Figure 5a), and a broken-fan-shaped texture is seen in the twist-bend nematic phase (Figure 5b). In some of the mixtures, the N_{TB} phase also shows focal conic (Figure 5c) and rope-like textures (Figure 5d).

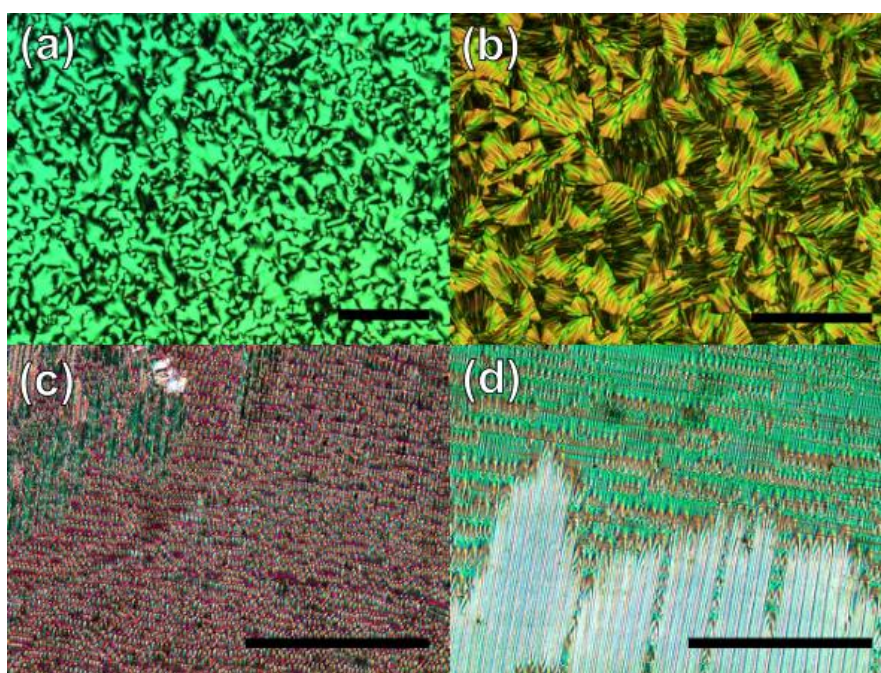


Figure 5

D. Dielectric properties

The plots in Figure 6 show the real part of the dielectric permittivity (ϵ') as a function of reduced temperature for a fixed frequency of 10 kHz. Closed symbols represent ϵ'_{\perp} (obtained by applying 0.1 V_{RMS} to the device) values and open symbols represent ϵ'_{\parallel} (obtained by applying 20 V_{RMS} to the device; for more information, see Experimental section); only the isotropic and nematic phases are labelled. Figure 6a is the permittivity data for pure 5CB and mixtures **M50**, **M60** and **M75**, and these materials show only the nematic phase (no N_{TB} phase) until room temperature. The dielectric permittivity data for the mixtures which show the N_{TB} phase in addition to the nematic phase is split into two plots for clarity, which are given in Figure 6b and Figure 6c.

Pure 5CB and the two mixtures **M60** and **M75** that only show the nematic phase have similar isotropic permittivities, as shown in Figure 6a. On cooling from the isotropic phase, in the nematic phase, ϵ'_{\perp} (closed symbols) decreases for all binary mixtures and pure materials (all three plots given in Figure 6), whereas ϵ'_{\parallel} (open symbols) increases in Figures 6a,b. This indicates a positive dielectric anisotropy for the materials in their nematic phase across the temperature range. On the other hand, the pure CB7CB and the mixtures **M10**, **M25** and **M30** show a decrease in ϵ'_{\parallel} with decreasing temperature in the nematic phase (Figure 6c). More details are provided later. With respect to the permittivity in the N_{TB} phase, for binary mixtures having a lower concentration of 5CB, i.e. **M10**, **M25** and **M30**, a significant drop in ϵ'_{\parallel} is observed close to the N to N_{TB} phase transition (Figure 6c).

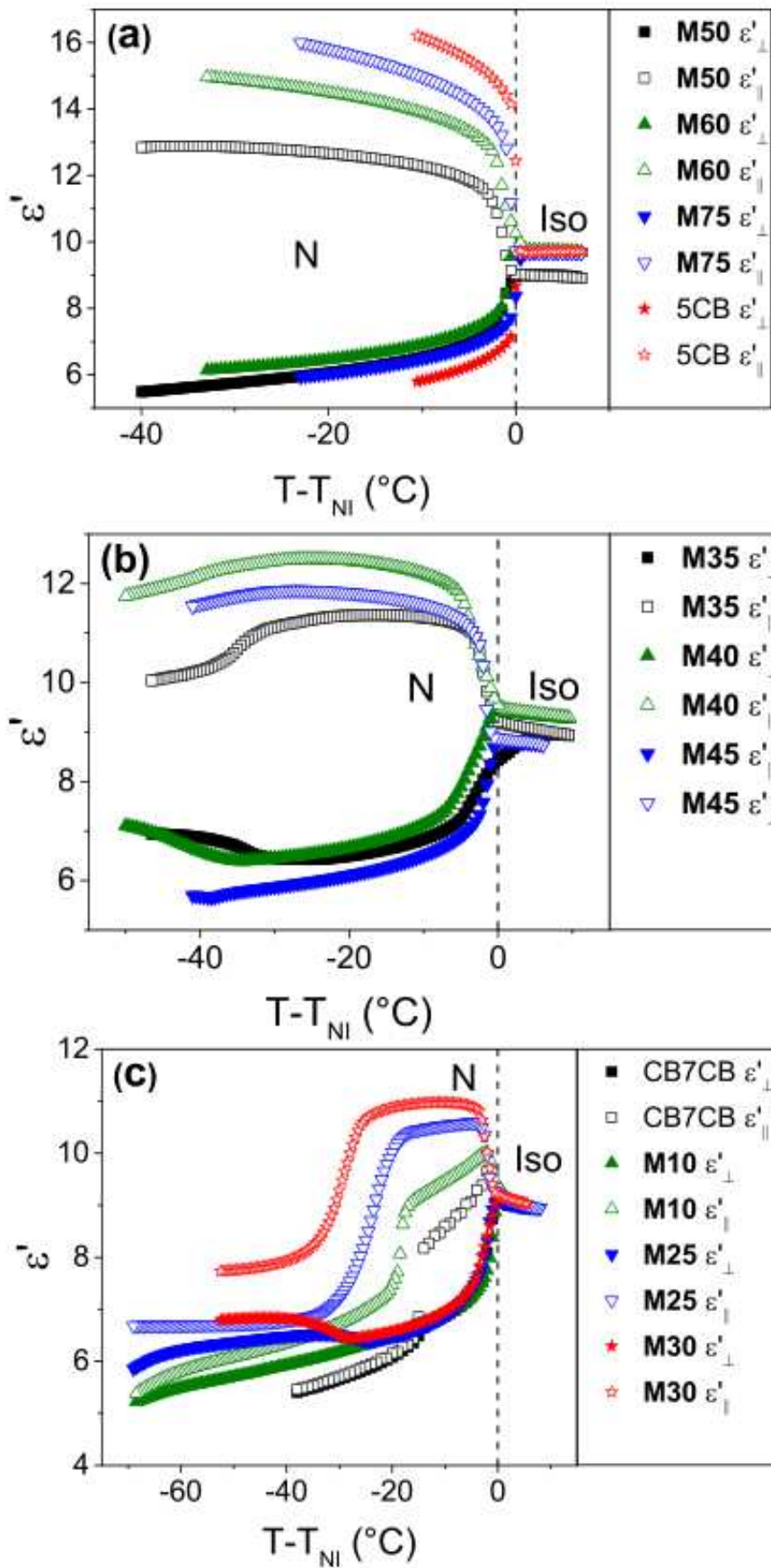


Figure 6

A plot of dielectric permittivity (ϵ'_{\perp} and ϵ'_{\parallel}) as a function of concentration for a fixed temperature of $T-T_{NI} = -5^{\circ}\text{C}$ is shown in Figure 7a. On increasing the concentration of 5CB, ϵ'_{\parallel} increases linearly by a considerable amount, from 9.08 for pure CB7CB to 15.48 for pure 5CB. The slope of the linear fit is 0.066. In contrast to this, the values of ϵ'_{\perp} do not change significantly; instead, they show a slight decrease from being 7.25 in pure CB7CB, to 6.25 in pure 5CB. The change in permittivity in the nematic and twist-bend nematic phases results in a considerable deviation in the average permittivity from the isotropic phase (details discussed later). Figure 7b shows the dielectric anisotropy ($\Delta\epsilon$) as a function of the concentration of 5CB at $T-T_{NI} = -5^{\circ}\text{C}$ in the nematic phases of the liquid crystals. Clearly, as more 5CB is added to the dimer, $\Delta\epsilon$ increases linearly from 1.24 (in pure CB7CB), to 7.41 (in the 75 wt% 5CB mixture). The slope of linear fit is 0.079.

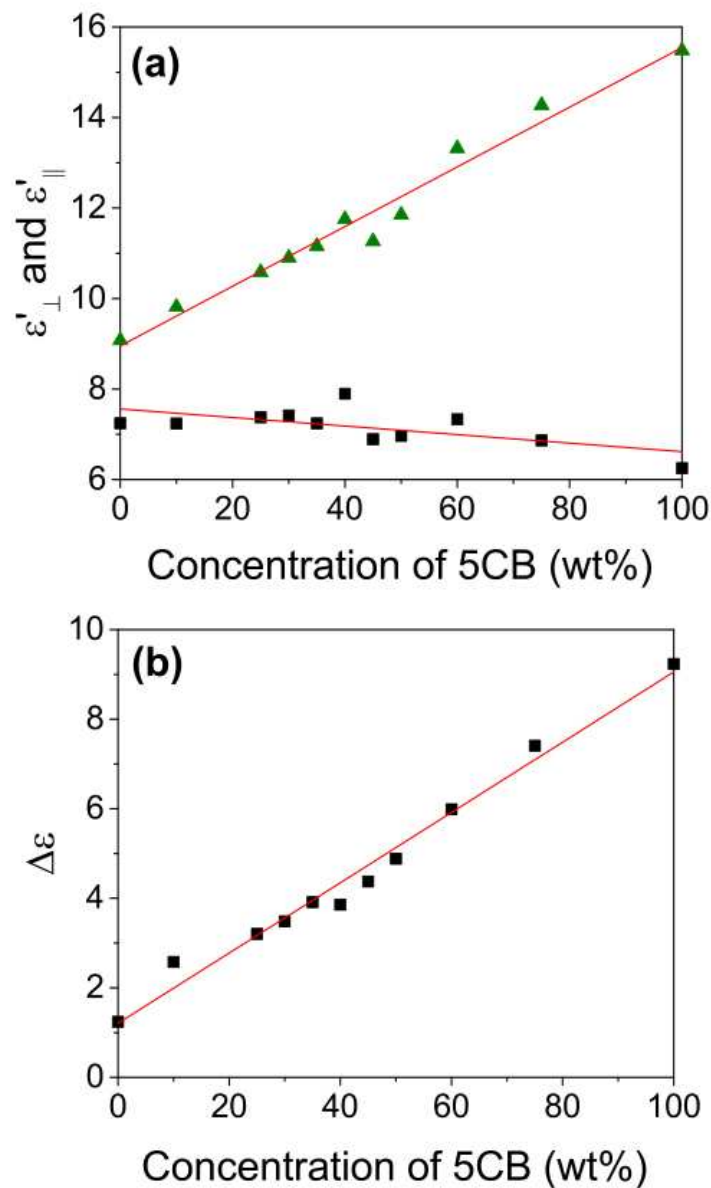


Figure 7

Assuming cylindrical symmetry of the liquid crystals, the average dielectric permittivity is calculated as an average of the permittivity contributions measured along the two molecular axes: $\varepsilon'_{average} = (\varepsilon_{\parallel} + 2\varepsilon_{\perp})/3$. Figures 8a-d show plots of the real part of the dielectric permittivity and the average value as a function of temperature. Figure 8a corresponds to **M25** – a mixture which exhibits the nematic and N_{TB} phases, and Figure 8b corresponds to **M50** – a mixture which exhibits only the nematic phase. Dielectric permittivity plots for pure CB7CB and 5CB have also been presented for comparison in Figure 8c and Figure 8d, respectively. In pure cyanobiphenyls, a decrease in $\varepsilon'_{average}$ at the nematic to isotropic transition has been attributed to the antiparallel correlation of the dipole moment in the nematic phase of the liquid crystals. Likewise, a decrease in the average dielectric permittivity at the isotropic to nematic phase transition in cyanobiphenyl-based odd dimers (dimers having an odd number of alkyl units in the spacer chain) has been observed before [30]. Such behaviour has been attributed to a shift in the distribution of the conformer population at the isotropic to nematic phase transition. Specifically, a significant decrease of $\varepsilon'_{average}$ in pure dimeric liquid crystals indicates an increase in the average number of bent conformers. In general, the reduction in $\varepsilon'_{average}$ suggests a strong decrease in the mean-square dipole moment upon cooling from the isotropic state. The cyanobiphenyl-based dimers with an odd number of spacer units exhibit bent and hairpin conformations. The bent conformers have a zero mean-square dipole moment if the angle between the terminal dipoles is greater than 90° . This gives rise to a non-zero contribution to the orientational dielectric permittivity. In contrast, hairpin conformers have a small angle between the terminal polar groups, resulting in a large mean-square dipole contribution to ε'_{\parallel} , and hence to $\varepsilon'_{average}$. Now, in case of the binary mixtures of CB7CB+5CB liquid crystals, the mixture **M50** (Figure 8b), which only exhibits the nematic phase, behaves in a similar way to pure 5CB (Figure 8d), showing very little change in the average dielectric permittivity across the temperature range of the isotropic and nematic phase (Figure 8b, open triangles). On the other hand, the mixture **M25** (Figure 8a) shows a significant reduction in $\varepsilon'_{average}$, which is similar to the behaviour of pure CB7CB (Figure 8c). It should be noted that at lower temperatures in the N_{TB} phase of CB7CB the $\Delta\varepsilon$ reduces considerably and becomes zero indicating the possibility of dual frequency responses. Whereas, in the N_{TB} phase of the binary mixtures, the $\Delta\varepsilon$ remains positive throughout the temperature range. It should also be noted that permittivity measurements given here correspond to a frequency of 10 kHz as opposed to permittivities obtained in the range 10^6 to 1.8×10^9 Hz in reference [4]. A plot of average permittivity as a function of reduced temperature for a set of binary mixtures is given in Figure 8e. Closed symbols represent mixtures that only exhibit the nematic phase and open symbols represent mixtures with both the nematic and N_{TB} phases. As the temperature decreases, the mixtures which form the N_{TB} phase (**M10**, **M30** and **M40**) show a clear reduction in the average dielectric permittivity. Figure 8f shows the average permittivity as a function of concentration at various temperatures below T_{NI} . A linear increase in $\varepsilon'_{average}$ as a function of composition is seen for binary mixtures exhibiting the twist-bend nematic phase (0 – 40 wt% 5CB), with $\varepsilon'_{average}$ increasing from 7.77 for pure CB7CB to 9.07 for the 40 wt% mixture, where both values correspond to $\varepsilon'_{average}$ at $T - T_{NI} = -6^\circ\text{C}$. The $\varepsilon'_{average}$ values for the 45 wt% and 50 wt% 5CB mixture further decrease compared to the 40 wt% mixture, and then there is a

sudden increase in value for the 60 wt% 5CB mixture. The 60 wt% and 75 wt% mixtures have average permittivities very similar to those of pure 5CB.

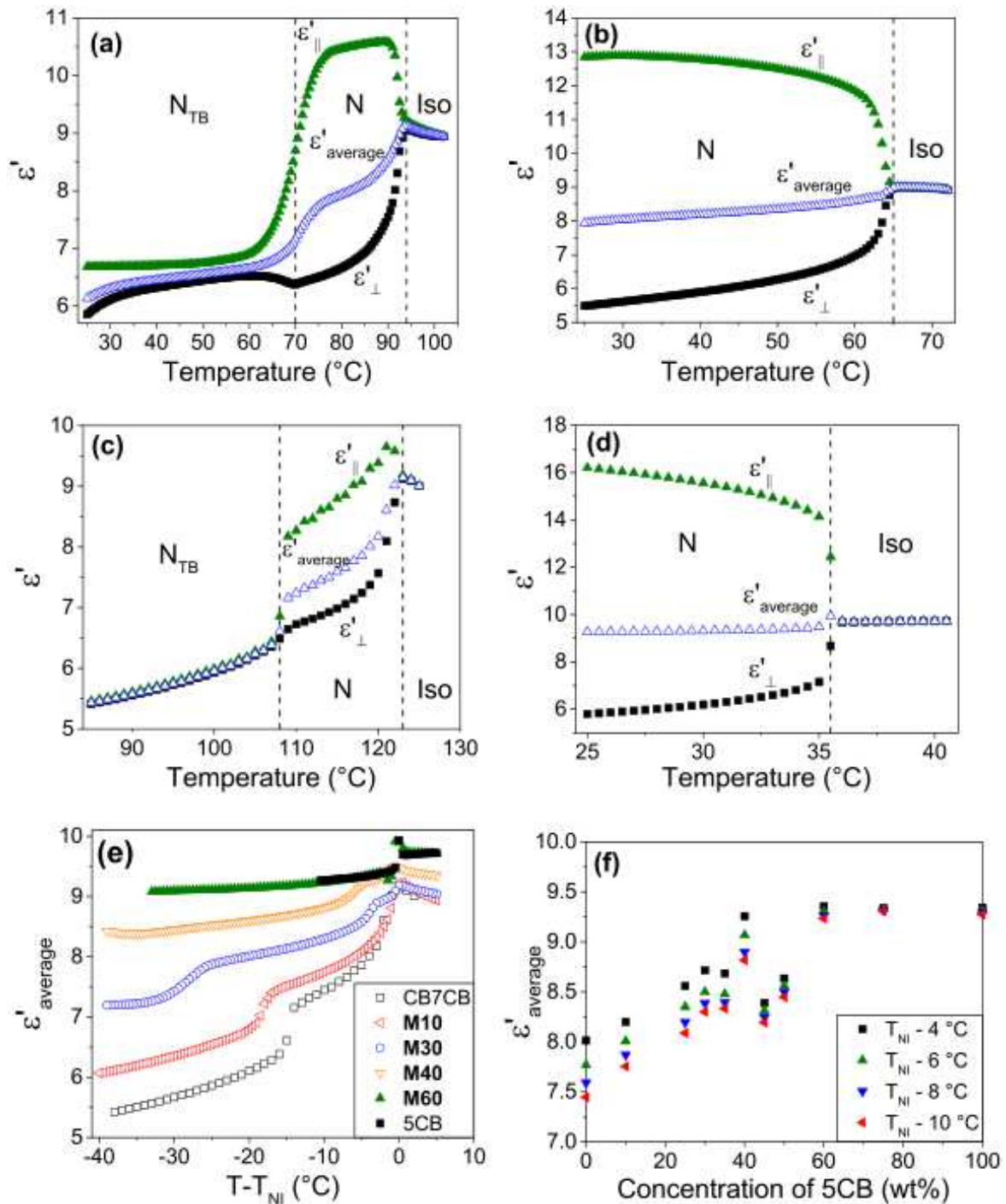


Figure 8

The imaginary part of the dielectric permittivity (ϵ'') is measured as a function of frequency for all binary mixtures and pure materials in planar and homeotropic devices. In a planar device, for pure 5CB and mixtures exhibiting only the nematic phase, such as **M50**, **M60** and **M75**, no relaxation peak was observed within the measured frequency window. In

contrast, for pure CB7CB and for mixtures having the N_{TB} phase, a single relaxation peak (P1) was observed in both planar ($P1_{\perp}$) and homeotropic ($P1_{\parallel}$) device geometries at temperatures corresponding to the N_{TB} phase, apart from the mixture **M45** in a planar device. A representative plot of the imaginary part of dielectric permittivity as a function of frequency for the binary N_{TB} mixture **M25** is given in Figure 9. As the sample is cooled from the isotropic state, no relaxations were observed in the frequency range 1 kHz to 2 MHz in the nematic phase, however, a relaxation peak ($P1_{\perp}$) appears close to the nematic to twist-bend nematic phase transition. On further cooling the sample, $P1_{\perp}$ shifts to lower frequencies, falling between the $10^4 - 10^5$ Hz frequency range at ~ 25 °C (marked with a box in Figure 9). In homeotropic devices with ϵ'' results similar to those in planar devices, as the concentration of 5CB increases, a single relaxation peak, $P1_{\parallel}$ was observed for mixtures **M10** – **M45**.

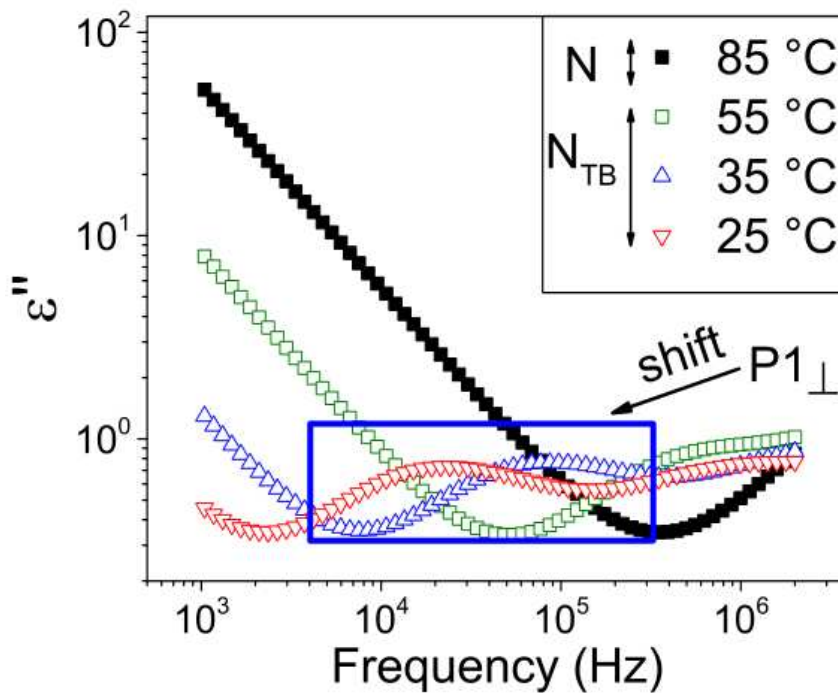


Figure 9

Further, the dielectric loss was fitted to the Havriliak-Negami equation [34] to obtain the relaxation frequencies (f_R) and dielectric strengths ($\delta\epsilon$) of peak P1. Both the relaxation frequency and dielectric strength of P1 for CB7CB and all binary mixtures in which the N_{TB} phase is observed are given as a function of reduced temperature in Figure 10. Figures 10a,b show the relaxation frequency and dielectric strength of $P1_{\perp}$ and Figures 10c,d show the same for $P1_{\parallel}$. The lowest temperature at which dielectric properties are measured ranges between 25 – 45 °C, hence the temperature windows given in Figure 10 vary. The most important feature to note is that relaxation frequencies of the dimer and all binary mixtures given in Figures 10a,c (**M10** – **M45**, irrespective of the alignment of the director) decrease as the temperature is lowered. The dielectric strength given in Figures 10b,d generally increases as the temperature decreases and also tends to increase in value as the concentration of 5CB increases. However, in Figure 10b the dielectric strength of $P1_{\perp}$ in pure CB7CB (square

symbols) shows a slight decrease (at $T-T_{N-N_{TB}} = -28$ °C, $\delta\varepsilon = 0.11$ and at $T-T_{N-N_{TB}} = -58$ °C, $\delta\varepsilon = 0.095$). The measurability of the relaxation peak cannot be linked to frequency, as the relaxation peak emerges at varying frequencies for certain mixtures. For example in Figure 10c, **M25** becomes measurable at a higher frequency than **CB7CB**, but also has a smaller frequency window compared to **CB7CB**. A link could be made between the concentration of 5CB in the mixtures and the temperature at which $P1_{\perp}$ emerges in the measurable frequency window in Figure 10a – as the concentration of 5CB decreases, the temperature at which $P1_{\perp}$ becomes measurable shifts further away from the $N-N_{TB}$ phase transition. For example, peak $P1_{\perp}$ becomes measurable for mixture **M35** at $T-T_{N-N_{TB}} = -5$ °C and for **CB7CB** at $T-T_{N-N_{TB}} = -28$ °C. The 45 wt% mixture **M45** in Figure 10c shows $P1_{\parallel}$ in the nematic phase as well as in the N_{TB} phase, close to the $N-N_{TB}$ transition; the boundary between the nematic and twist-bend nematic phases is represented with a vertical, dashed line on the graph. A sudden drop in the relaxation frequency at the $N-N_{TB}$ phase boundary of **M45** (circle symbols) can be seen.

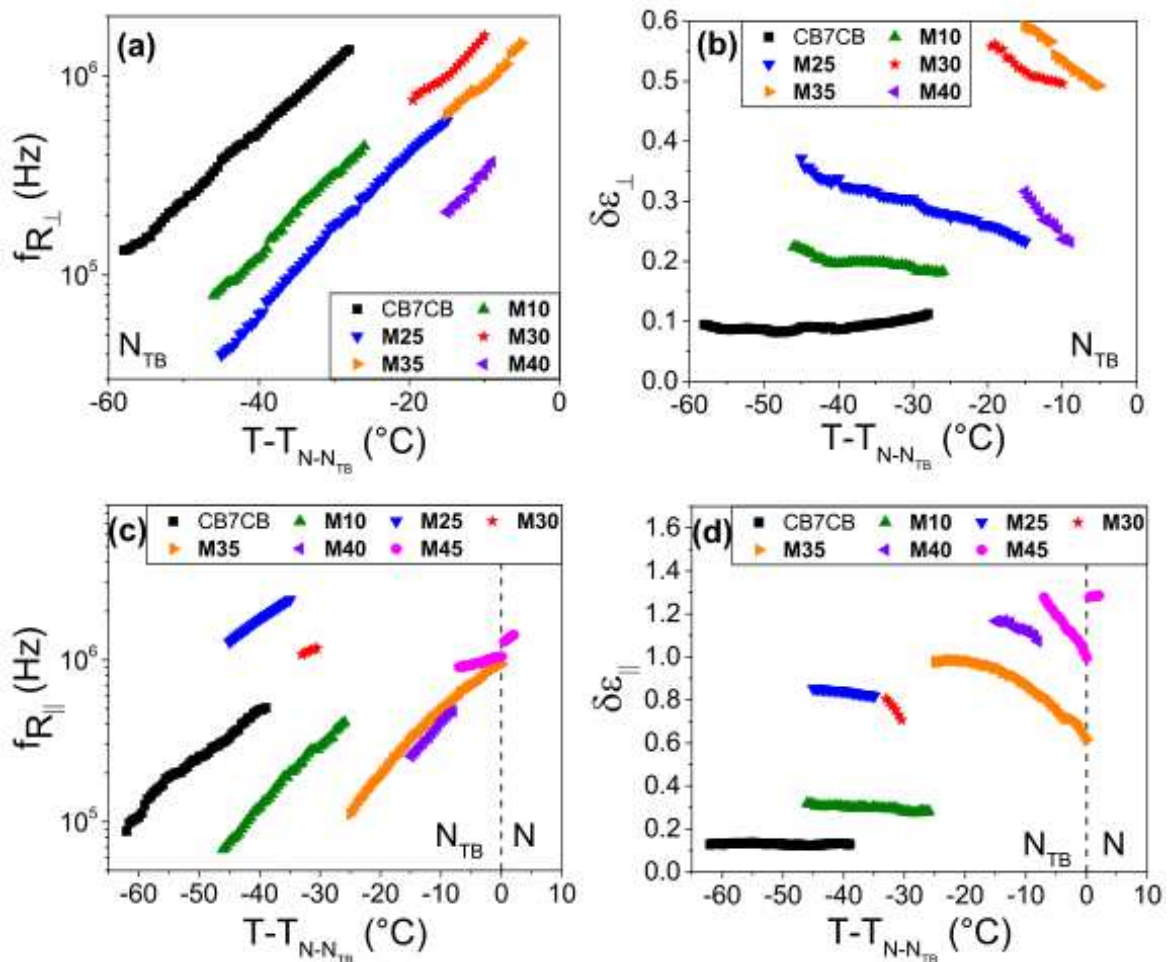


Figure 10

The dipole moment of the nematic and twist-bend nematic phases of **CB7CB** results in two relaxation modes involving rotational dynamics: an end-over-end or flip-flop motion of

the dipoles parallel to the director and a precessional motion of the dimer's dipole groups units about the director. For the pure dimer and binary mixtures studied in perpendicular and homeotropic devices, the relaxation peak P1 shifts towards lower frequencies on cooling, as seen in Figures 10a,c. This relaxation can be correlated to the flip-flop motion of the dipolar groups parallel to the director, as seen in previous studies for CB7CB [4], CB9CB [24] and BCB.O11 [27].

To understand the relationship between activation energy of the relaxation process P1 and the concentrations of liquid crystals, the temperature dependence of relaxation frequencies are fitted to the Arrhenius equation. A plot of \log_{10} values of relaxation frequencies as a function of the inverse of temperature ($1/T$) of P1 for the 25 wt% 5CB mixture **M25** is given in Figure 11a. Figure 11b shows \log_{10} values of relaxation frequencies as a function $1/T$ for mixtures **M10** – **M40** that exhibit the N_{TB} phase. Activation energies (E_a) of P1 in the N_{TB} phase are calculated from the gradient of the plot and are given in Figure 11c as a function of the concentration of 5CB, where errors calculated from the linear fitting are also included. The graph in Figure 11c shows that for perpendicular alignment of the director (square symbols) the 40 wt% mixture has $E_a = 31.90 \pm 1.09 \text{ kJ mol}^{-1}$ and the activation energy of pure CB7CB ($32.90 \text{ kJ mol}^{-1}$) fits within the error of the measurements for the 40 wt% mixture. This implies that for all binary N_{TB} mixtures, the activation energy remains almost constant. The 25 wt% and 30 wt% of 5CB mixtures in homeotropic devices both clearly deviate in comparison to their planar devices (Figures 11b,c). For the 25 wt% mixture in a planar device $E_a = 32.62 \text{ kJ mol}^{-1}$, and in a homeotropic device $E_a = 19.92 \text{ kJ mol}^{-1}$. For the 30 wt% mixture in a planar device $E_a = 27.22 \text{ kJ mol}^{-1}$, whereas for the homeotropic device $E_a = 12.07 \text{ kJ mol}^{-1}$. This could be due to the fact that for these two mixtures, the activation energies in homeotropic devices were calculated for a data set at a smaller temperature window compared to the planar devices – in Figure 11b, for the 30 wt% mixture, $P1_{\parallel}$ is observed only across a 2.5 °C temperature window. It is also noted that the activation energies of the 10 wt% 5CB and the 40 wt% 5CB have very similar values in both perpendicular and homeotropic devices.

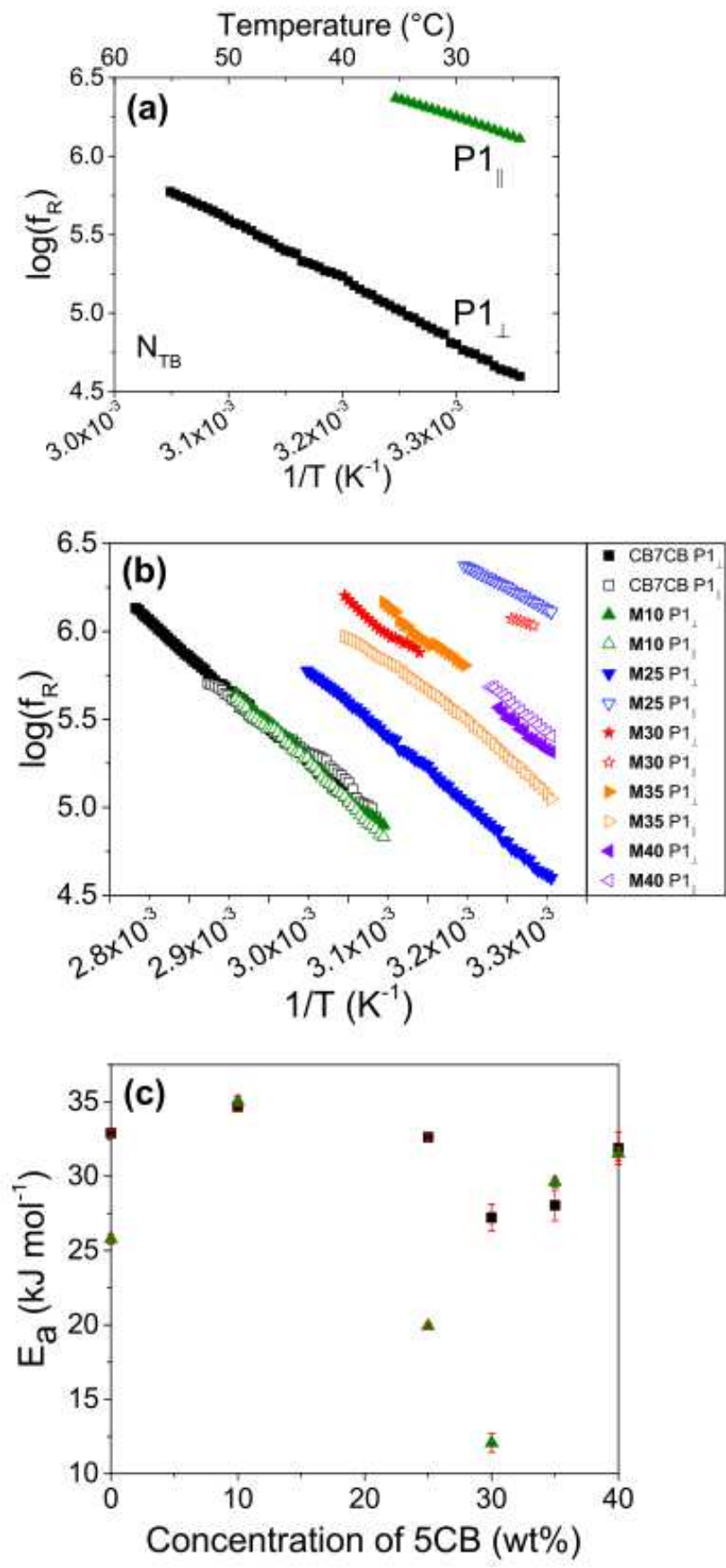


Figure 11

IV. CONCLUSIONS

A detailed investigation of the thermal and dielectric properties of a series of binary mixtures exhibiting the nematic and twist-bend nematic liquid crystal phases has been presented, with the aim to understand the influence of the calamitic liquid crystal 5CB on phase transition temperatures, the stability of the N_{TB} phase and the dielectric properties of the dimeric liquid crystal. A phase diagram of the two-component system is presented in Figure 3, which shows features such as a linear decrease in the phase transition temperatures of the binary mixtures and an increase in the width of the nematic phase, both as the concentration of the calamitic liquid crystal is increased. Differential scanning calorimetry measurements were undertaken to calculate enthalpies of transitions, and to understand the nature of the N to N_{TB} phase transition. Compared to a first order transition seen in the pure dimer (with $\Delta S/R = 0.38$), an increase in the concentration of the calamitic liquid crystal resulted in a significant decrease in the associated energies of the N- N_{TB} phase transitions. No measurable enthalpies could be obtained for the N- N_{TB} transition when the concentration of 5CB was increased beyond 30 wt%, even though these mixtures showed a sharp transition between the nematic schlieren texture to the focal conic and rope-like textures of the twist-bend nematic phase when observed by polarising optical microscopy.

The measurement of the real and imaginary parts of the dielectric permittivity for both planar and homeotropic alignment of the liquid crystal in the nematic and N_{TB} phases of the binary mixtures showed two important features. The first was a significant decrease in the average dielectric permittivity as a function of temperature for mixtures forming the N_{TB} phase (see Figure 8e). Interestingly, this decrease was seen even in the nematic phase, prior to the N_{TB} transition. The second important feature was the observation of a single relaxation peak for all binary mixtures exhibiting the N_{TB} phase, which emerged in the N_{TB} phase and on decreasing the temperature shifted towards lower frequencies (in the $10^4 - 10^5$ Hz range). A combination of these two features could be used to indicate the presence of a twist-bend nematic phase in the absence of polarising optical microscopy and DSC measurements. Relaxation frequencies (f_R) for all binary CB7CB/5CB mixtures and pure materials decreased on cooling from the isotropic state. The relaxation peak correlated to the flip-flop motion of the dipolar groups parallel to the director. The relaxation frequencies were fitted to the Arrhenius equation from which activation energies of mixtures exhibiting the twist-bend nematic phase were calculated. No significant variation in the activation energy was observed as the 5CB concentration was changed in the binary mixtures.

V. References

- [1] V. P. Panov, M. Nagaraj, J. K. Vij, Y. P. Panarin, A. Kohlmeier, M. G. Tamba, R. A. Lewis, G. H. Mehl, Phys. Rev. Lett. **105**, 167801 (2010).
- [2] V. P. Panov, R. Balachandran, M. Nagaraj, J. K. Vij, M. G. Tamba, A. Kohlmeier, G. H. Mehl, Appl. Phys. Lett. **99**, 261903 (2011).

- [3] R. J. Mandle, E. J. Davis, C. T. Archbold, S. J. Cowling, J. W. Goodby, *J. Mater. Chem. C* **2**, 556–566 (2014).
- [4] M. Cestari et al., *Phys. Rev. E* **84**, 31704 (2011).
- [5] M. Šepelj, A. Lesac, U. Baumeister, S. Diele, H. L. Nguyen, D. W. Bruce, *J. Mater. Chem.* **17**, 1154–1165 (2007).
- [6] V. Borshch, Y.-K. Kim, J. Xiang, M. Gao, A. Jáklí, V. P. Panov, J. K. Vij, C. T. Imrie, M. G. Tamba, G. H. Mehl, et al., *Nat. Commun.* **4**, 2635 (2013).
- [7] R. Balachandran, V. P. Panov, Y. P. Panarin, J. K. Vij, M. G. Tamba, G. H. Mehl, J. K. Song, *J. Mater. Chem. C* **2**, 8179–8184 (2014).
- [8] D. O. López, N. Sebastian, M. R. de la Fuente, J. C. Martínez-García, J. Salud, M. A. Pérez-Jubindo, S. Diez-Berart, D. A. Dunmur, G. R. Luckhurst, *J. Chem. Phys.* **137**, 34502 (2012).
- [9] D. A. Paterson et al., *Soft Matter* **12**, 6827–6840 (2016).
- [10] C. S. P. Tripathi, P. Losada-Pérez, C. Glorieux, A. Kohlmeier, M.-G. Tamba, G. H. Mehl, J. Leys, *Phys. Rev. E* **84**, 41707 (2011).
- [11] M. R. Tuchband et al., *ArXiv Prepr. ArXiv151107523* (2015).
- [12] D. Chen, J. H. Porada, J. B. Hooper, A. Klittnick, Y. Shen, M. R. Tuchband, E. Korblova, D. Bedrov, D. M. Walba, M. A. Glaser, et al., *Proc. Natl. Acad. Sci.* **110**, 15931–15936 (2013).
- [13] C. Meyer, G. R. Luckhurst, I. Dozov, *J. Mater. Chem. C* **3**, 318–328 (2015).
- [14] I. Dozov, *EPL Europhys. Lett.* **56**, 247 (2001).
- [15] C. Greco, G. R. Luckhurst, A. Ferrarini, *Soft Matter* **10**, 9318–9323 (2014).
- [16] J. P. Jokisaari, G. R. Luckhurst, B. A. Timimi, J. Zhu, H. Zimmermann, *Liq. Cryst.* **42**, 708–721 (2015).
- [17] R. B. Meyer, *Phys. Rev. Lett.* **22**, 918 (1969).
- [18] C. Meyer, G. R. Luckhurst, I. Dozov, *Phys. Rev. Lett.* **111**, 67801 (2013).
- [19] A. Varanytsia, L.-C. Chien, *Sci. Rep.* **7**, 41333 (2017).
- [20] P. A. Henderson, C. T. Imrie, *Liq. Cryst.* **38**, 1407–1414 (2011).
- [21] K. Adlem, M. Čopič, G. R. Luckhurst, A. Mertelj, O. Parri, R. M. Richardson, B. D. Snow, B. A. Timimi, R. P. Tuffin, D. Wilkes, *Phys. Rev. E* **88**, 22503 (2013).
- [22] D. Chen, M. Nakata, R. Shao, M. R. Tuchband, M. Shuai, U. Baumeister, W. Weissflog, D. M. Walba, M. A. Glaser, J. E. MacLennan, et al., *Phys. Rev. E* **89**, 22506 (2014).
- [23] S. P. Sreenilayam, V. P. Panov, J. K. Vij, G. Shanker, *Liq. Cryst.* **44**, 244–253 (2016).
- [24] B. Robles-Hernández, N. Sebastián, M. R. de la Fuente, D. O. López, S. Diez-Berart, J. Salud, M. B. Ros, D. A. Dunmur, G. R. Luckhurst, B. A. Timimi, *Phys. Rev. E* **92**, 62505 (2015).
- [25] S. Parthasarathi, D. S. S. Rao, N. B. Palakurthy, C. V. Yelamaggad, S. Krishna Prasad, *J. Phys. Chem. B* **120**, 5056–5062 (2016).
- [26] G. Cukrov, Y. Mosaddeghian Golestani, J. Xiang, Y. A. Nastishin, Z. Ahmed, C. Welch, G. H. Mehl, O. D. Lavrentovich, *Liq. Cryst.* **44**, 219–231 (2016).
- [27] D. A. Dunmur, G. R. Luckhurst, M. R. de la Fuente, S. Diez, M. A. Pérez Jubindo, *J. Chem. Phys.* **115**, 8681–8691 (2001).
- [28] M. Stocchero, A. Ferrarini, G. J. Moro, D. A. Dunmur, G. R. Luckhurst, *J. Chem. Phys.* **121**, 8079 (2004).
- [29] D. A. Dunmur, M. R. de la Fuente, M. A. Perez Jubindo, S. Diez, *Liq. Cryst.* **37**, 723–736 (2010).
- [30] N. Sebastián, B. Robles-Hernández, S. Diez-Berart, J. Salud, G. R. Luckhurst, D. A. Dunmur, D. O. López, M. R. de la Fuente, *Liq. Cryst.* **44**, 177–190 (2017).
- [31] D. A. Dunmur, *Liq. Cryst.* **32**, 1379–1387 (2005).
- [32] N. Sebastián, M. R. de la Fuente, D. O. López, M. A. Pérez-Jubindo, J. Salud, S. Diez-Berart, M. B. Ros, *J. Phys. Chem. B* **115**, 9766–9775 (2011).

- [33] N. Sebastián, D. O. López, B. Robles-Hernández, M. R. de la Fuente, J. Salud, M. A. Pérez-Jubindo, D. A. Dunmur, G. R. Luckhurst, D. J. B. Jackson, *Phys. Chem. Chem. Phys.* **16**, 21391–21406 (2014).
- [34] S. Havriliak, S. Negami, *Polymer* **8**, 161–210 (1967).
- [35] See Supplemental Material at [URL will be inserted by publisher] for DSC curves of pure materials and mixtures M35, M40 and M50.
- [36] V. P. Panov, J. K. Vij, G. H. Mehl, *Liq. Cryst.* **44**, 147–159 (2016).
- [37] D. A. Paterson, J. P. Abberley, W. T. Harrison, J. M. Storey, C. T. Imrie, *Liq. Cryst.* **44**, 127–146 (2017).

Figure captions

Figure 1: Schematic representation of the twist-bend nematic phase in a liquid crystal dimer: p_{TB} represents the pitch of the helix, consisting of only a few molecules; θ represents the tilt angle; \mathbf{n} and \mathbf{h} are the direction of the director and the helical axis, respectively.

Figure 2: Chemical structures of 1'',7''-bis(4-cyanobiphenyl-4'-yl) heptane (CB7CB) and 4-cyano-4'-pentylbiphenyl (5CB) liquid crystals.

Figure 3: Gibbs phase diagram of the binary mixtures of 5CB and CB7CB liquid crystals obtained by polarising optical microscopy. The diagram shows the effect of varying the concentration of 5CB liquid crystal on the phase transition temperatures of the mixtures.

Figure 4: Plot of the enthalpy and entropy (inset) of phase transitions of the binary mixtures as a function of concentration. Squares represent isotropic to nematic transitions and triangles present nematic to N_{TB} transitions.

Figure 5: POM images of the CB7CB liquid crystal showing: (a) the schlieren texture in the nematic phase at $T-T_{NI} = -2$ °C, and (b) the broken-fan-shaped texture of the N_{TB} phase at $T-T_{N-N_{TB}} = -2$ °C. POM images of: (c) the focal conic texture of the N_{TB} phase of **M35** at $T-T_{N-N_{TB}} = -13$ °C, and (d) the rope-like texture of the N_{TB} phase of **M45** at $T-T_{N-N_{TB}} = -4$ °C. For (a), (c) and (d) the length of scale bar is 300 μm , whereas for (b) the scale bar is 100 μm .

Figure 6: Plots of the real part of the dielectric permittivity (ϵ') as a function of reduced temperature for both perpendicular (ϵ'_{\perp}) and homeotropic (ϵ'_{\parallel}) alignment of the director at a fixed frequency of 10 kHz for: a) 5CB, **M50**, **M60**, **M75**; b) **M35**, **M40**, **M45**; c) CB7CB, **M10**, **M25**, **M30**. Closed symbols represent ϵ'_{\perp} and open symbols represent ϵ'_{\parallel} .

Figure 7: Plots of: (a) ϵ'_{\parallel} (triangles) and ϵ'_{\perp} (squares) at $T_{NI} - 5$ °C, and (b) dielectric anisotropy ($\Delta\epsilon$) as a function of concentration at $T = T_{NI} - 5$ °C and $f = 10$ kHz. The lines represent linear fits to the data set.

Figure 8: Plots of parallel (ϵ'_{\parallel}), perpendicular (ϵ'_{\perp}) and average permittivity ($\epsilon'_{\text{average}}$) at 10 kHz measured over temperatures of the isotropic, nematic and twist-bend nematic phases for: (a) **M25**; (b) **M50**; (c) CB7CB; (d) pure 5CB. Plots of the average permittivity ($\epsilon'_{\text{average}}$) for mixtures and pure material: (e) as a function of reduced temperature in the N and N_{TB} phases, and (f) as a function of concentration of 5CB in the nematic phase.

Figure 9: Plots of the imaginary part of dielectric permittivity (ϵ'') as a function of frequency in the mixture **M25** (25 wt% 5CB), measured in a 10 μm planar cell.

Figure 10: (a) Relaxation frequency (f_R) as a function of reduced temperature for perpendicular alignment of the director; (b) dielectric strength ($\delta\epsilon$) a function of reduced temperature for perpendicular alignment of the director; (c) f_R for parallel alignment of the director; (d) $\delta\epsilon$ for parallel alignment of the director.

Figure 11: Relaxation frequency (f_R) as a function of $1/T$, for both perpendicular and parallel alignment of the director of: (a) **M25**; (b) mixtures **M10** – **M40** exhibiting the N_{TB} phase. (c) Activation energy (E_a) as a function of 5CB concentration for pure CB7CB and mixtures **M10** – **M40**. E_a is calculated for the N_{TB} phase and errors are obtained from linear fitting; squares and triangles represent activation energies for perpendicular and parallel alignment of the director, respectively.